Latin American Journal of Solids and Structures
www.lajss.org

Laboratory study of dynamic mechanical characteristic of granite subjected to confining pressure and cyclic blast loading

Abstract
To investigate the deformation characteristic of deep rock under cyclic blasting, the static-dynamic loading experimental equipment was set up. The dynamic strain gauges and high-speed (HS) camera were adopted to obtain strain field and the crack propagation of rock under confining pressure of 0 MPa, 5 MPa and 10 MPa. Under the one-time loading from cylindrical charge, the cracks in crushed zone were generated by shear and tensile failure. Circumference compressive stress is formed around borehole by confining pressure, and it reduces the circumference tensile failure by blast loading. The number of radial cracks and broken radius reduce with confining pressure increase. The reflected stress wave drives the existing fissures further developing. When specimens subjected to cyclic loading from PETN Cord, the rock is controlled by elastic deformation and no damage appeared after the first loading. With the cycle-index increase, the accumulation of plastic strain is observably when the strain exceeds the elastic limit strength of rock. The cumulative damage is nonlinear increased under cyclic loadings. The existing flaws or radial cracks run through specimen when the cumulative damage exceeds the material's yield strength.

Keywords
Rock mechanics; cyclic blast loading; confining pressure; deformation characteristic; damage accumulative evolution.

Chenglong He[a]*
Jun Yang[b]

[a] College of Mechatronics Engineering, North University of China, Taiyuan 030051, China. E-mail: hechenglong@bit.edu.cn

[b] State Key Laboratory of Explosion Science and Technology, Beijing Institute of Technology, Beijing, China. E-mail: yangj@bit.edu.cn

*Corresponding Author

https://doi.org/10.1590/1679-78254424

Received August 23, 2017
In revised form November 22, 2017
Accepted December 08, 2017
Available online February 02, 2018

1 INTRODUCTION

With the increasing of deep tunnel engineering and underground resources exploitation, the dynamic response of deep rock subjected to the cyclic blast loading becomes complicated. Unlike surface rock, underground rock located in the environment with high in-situ stress, for instance, the vertical in-situ stress rise up to 27 MPa at a depth of 1000 m and the horizontal part can be approximately 13.5 MPa (Brown & Hoek, 1978). When rock mass subjected to dynamic cyclical loading such as impact loading and blast loading, a few of micro cracks are generated after initial loading. Then micro cracks grow and merge each other under subsequent loading, the damage accumulation caused the material failure completely at last (Li et al., 2011; Ramulu, Chakraborty, & Sitharam, 2009). Under the action of static and cyclic blasting, the deformation behaviour and failure mechanisms of rock are complicated (Figure 1). Therefore, the study of dynamic mechanical characteristic and cumulative damage of deep rock under cyclic blasting is essential.

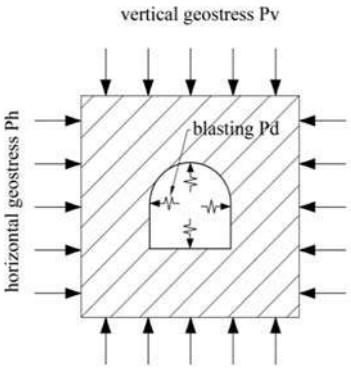

(cc) BY

Figure 1: Sketch of the loading state of underground rock.

The attenuation of shock wave from cylindrical charges has been investigated. The properties of the explosive, rock materials and coupling media would influence the failure process of rock. Generally, the explosion loading consists of shock waves and explosion gases, both of them play important place in the dynamic response of rock (Onederra, Furtney, Sellers, & Iverson, 2013). High Shock waves are generated initially and quickly spread to the borehole wall, the micro cracks appear due to shear band interconnection under extremely high pressures. As a result, the zone closed to the blast hole is crushed and pulverized. The tensile stress follow by compressive stress wave and drive the existing radial cracks developing. The fragmentation became more seriously by reflected waves along the boundary zone. Finally, the subsequent explosion gases flow into existing cracks, and then cracks run through specimen at last (Cho & Kaneko, 2004; Eason, 1963; E. L. Liu, He, Xue, & Xu, 2011; Rathore & Bhandari, 2007).

In previous studies, the MTS-815 rock test system, drop hammer experiment, and split hopkinson pressure bar (SHPB) were adopted to investigate the damage accumulate of rock under cyclic loading. When the loading was less than the threshold value of salt rock, three stages including initial deformation, constant velocity deformation and accelerating deformation were divided to describe the dynamic response process. Meanwhile the fatigue failure of salt rock was also controlled by static loading by confining pressure, and the axial strain and cycle-index at failure increased with the frequency by experimental study on MTS-815 test system (Guo et al., 2011; J. Liu, Xie, Xu, & Yang, 2008). The dynamic fatigue strength reduced with loading frequencies and amplitude, and the dynamic modulus increased with loading frequency (Bagde & Petroš, 2005).

Poisson's ratio was attributed to the dilatant and viscoelastic, and strain rates increased with an increase in the maximum applied stress (Ma et al., 2013). Lin, Chen, and Liu (2005) adopted the drop-weight test to analyze the confining pressure effect of rock, concluded the damaged by cyclical impact loading were obviously, and the existence of confining pressure also increased the ability of rock against impact damage.

For the SHPB experimental investigation, (Ge, Yu, Lu, & Ren, 2003) focused on the strain of fatigue failure corresponding to the maximal cyclic load, and reported the relation between the ability of resistance against cyclic impacts and cycle-index was from slow development to sharp decline. Wang, Xu, Liu, and Wang (2016) carried out the physical tests on red-sandstone free from and after 10, 20, 30, and 40 artificial TS cycles. The results showed that mineral loss and cement weakening lead to the increase of porosity and decrease of strength during the TS weathering process. The dynamical mechanical properties were improved with the increase of strain rate under impact loading. When the axial compression was 0, 65%, 87%, the ability of resistance against cyclic impacts dropped constantly during the whole cyclic loading (Jin, Xi-Bing, Yin, & Kun, 2012).

Although numerous studies were carried out on mechanical properties of rock under the coupled static and impact loads, these works were limited to test the dynamic behaviour of rock material under impact loading (SHPB or Drop-weight test). It is well-known that the strain rate of rock under blasting is higher than that of impact loading. The stress wave from blast loading is gradually reduced during propagation. Therefore, this paper adopted the cyclic blast loading and investigated the deformation behaviour and damage accumulation in granitic with different confining pressures (0 MPa, 5 MPa, 10 MPa). The dynamic strain gauges, high-speed cameras (HS) and digital image correlation (DIC) were used to quantify the dynamic response and observe crack propagation process. At first, the fracturing process with different confining pressures under one-time blast loading is studied. Then the failure process and damage accumulation of rock under the cyclic loading are investigated. Some useful conclusions are given at last.

2 EXPERIMENT

2.1 Rock materials

The rock samples in experiment were taken from the Fang Shan area (Beijing. China), and all samples were come from the same parent rock. According to the International Society for Rock Mechanics (ISRM) standards, the water drilling, friction sanding and polishing techniques were used to insure the accuracy of granite specimens. The specimens were carefully ground by a grinding machine to ensure that the parallelism between the top and bottom surface is within 0.1 mm. The microscopic tests were performed to observe the mineralogical composition and original microstructure by via scanning electron microscopy (SEM) in physical and chemical analysis test centre (Beijing, China). As shown in Figure 2, Fang Shan granite mainly consists of two parts, the light part mainly include barite, white mica and garnet, and the black part is magnetite. SiO_2 (47.75%) and CaO (8.16%) were mainly

component elements in Fang Shan granite. The properties parameters of granite were as follows: average density = 2.70 g/cm^3, Poisson's ratio = 0.23, P-wave velocity = 3738 m/s, Young's modulus = 40.6 GPa.

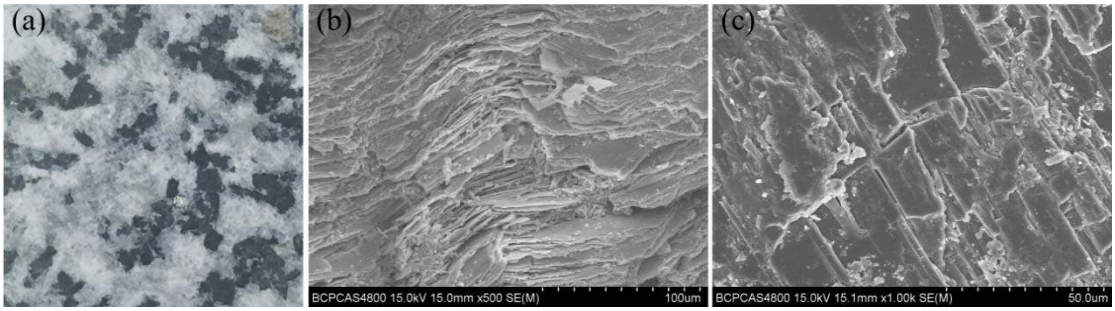

Figure 2: Specimens and SEM images. (a) Photograph of rock sample; (b) SEM on 100 μm; (c) SEM on 50 μm.

The quasi-static properties of granite were tested using the WDW-300 electronic universal testing machine in the Laboratory of Explosion at the Beijing Institute of Technology (Beijing, China). The cylindrical specimens were cut into Φ 50×25 mm and Φ 50×100 mm for tension and compression quasi-static test, respectively. The BX 120-4AA strain gages (sensitive grid size is 4×2 mm) were used to collect deformation during loading. The rock specimen was compressed at a speed of 0.2 mm/s and t strain signals were recorded on 2 /s. The stress-strain curves were given in Figure 3, the tensile strength of granite is 6 MPa (700 με) and compressive strength is 86 MPa (2100 με). Both the tensile and compressive stress curves drop sharply after stress reach the maximum stress, that indicate the brittle fracture should be responsible for the failure of granite specimens in quasi-static experiment.

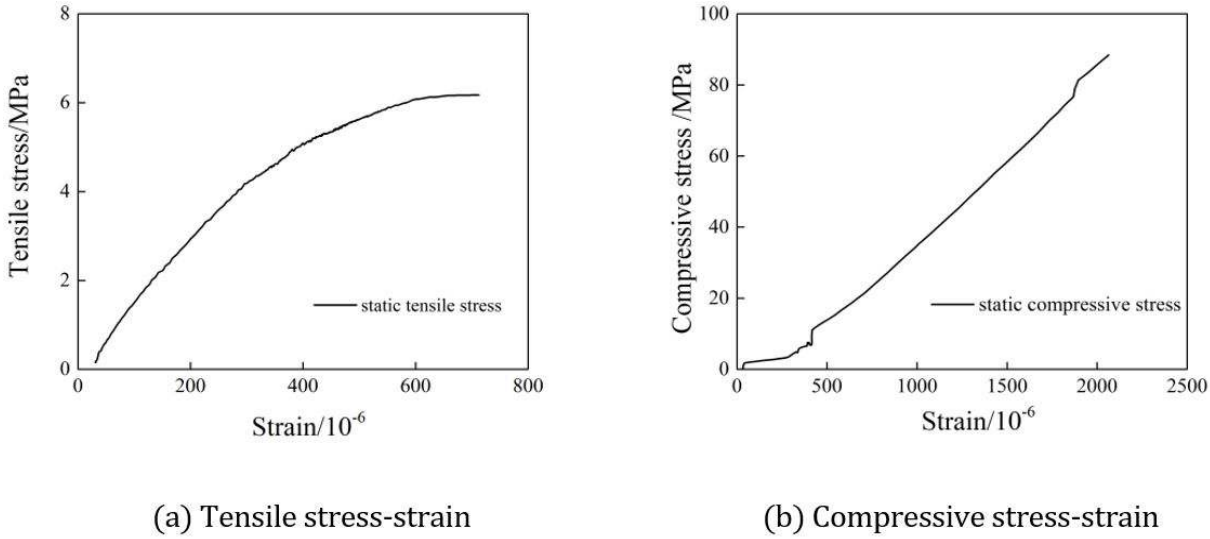

Figure 3: Stress-strain of FangShan granite in the quasi-static test results.

SHPB was a typical experiment for testing dynamic behavior of materials at nominal strain rates ranging from 100/s to 10 ^{4}/s, which has also been used for rock-like materials (Zhang & Zhao, 2014; Zhou, 1998). SHPB experiment was carried out for the granite with higher strain rate (approximately 100 /s) at China University of Mining and Technology (Beijing, China). All bars were 18Ni maraging steel to match the wave impedance of the rock samples with a diameter of 74 mm. BHF350-2AA strain gauges (sensitive grid size is 2.4×2 mm) were manufactured by Huangyan Instruments Co. China. The speed of striker bar was approximately 7 m/s and the strain signals were recorded by LTT24-Messsystem on 2 MS/s sampling rate. As shown in Figure 4, the dynamic compressive strength is 120 MPa and dynamic tensile strength is 8 MPa, the failure strain is 0.007 and 0.0015, respectively. Different from the brittle failure in quasi-static test results, the specimens were not failure immediately when the stress exceeds the yield strength. When the strain increased from 0.002 to 0.0075, compressive stress-strain oscillated near 120 MPa .

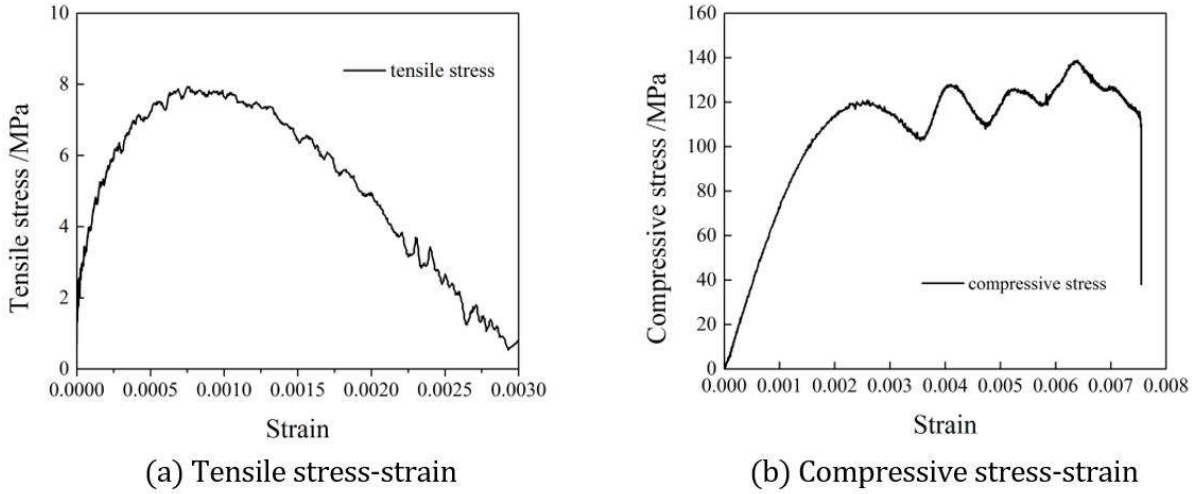

Figure 4: The dynamic stress-strain curves from SHPB results.

2.2 Test system and equipment

The experiment equipment mainly includes the servo pressure system, experimental platform and test system, as shown in Figure 5. In the first part, the hydraulic actuator provides pressure for jacks to simulate the in-situ stress conditions, the high-pressure oil pipe and pressure gage are used to control the pressure value accurately. The experimental platform consists of four correcting wedges, two jacks, four baseboards and outer frame. The pressure acted on the cylindrical specimen is uniformly by the correcting wedge. To observe crack growth and capture the dynamic deformation of rock, the High-speed camera and strain test are introduced, respectively. The strain field is calculated by VIC-2D base on the photographs from High-speed camera. The TTL signal is selected to trigger the camera and strain gauge simultaneously.

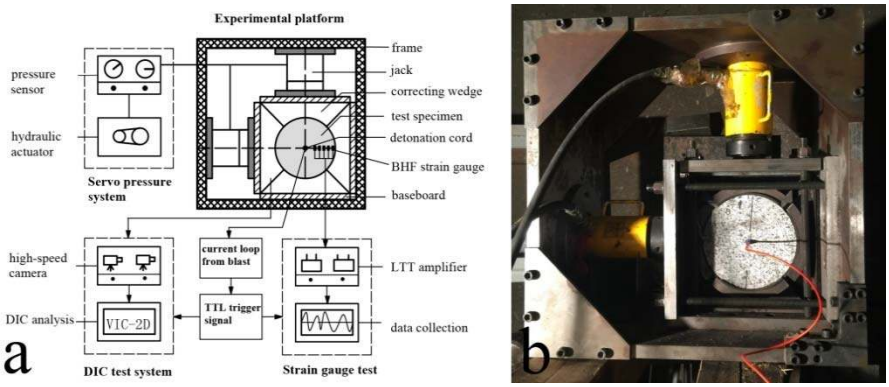

Figure 5: Schematic diagram of equipment. (a) Test system; (b) Photograph of experiment equipment.

Many factors should be considered before designing the experiment, such as the specimen geometry size, explosive types and uncoupling factors. The fragments and spall cracks caused by reflected tension waves should be removed from the free surface. Because the diffusion of explosion gas reduces the sharpness of photographs from HS, the nonpenetrative borehole was designed to prevent the explosion gas overflowing from the bottom of the borehole.

The selection of charge and specimen size can reference the previous experiment. Simha, Fourney, and Dick (1984) experimented with Plexiglas sheets (305×305×50 mm), and the PETN charge was 0.5 g and 10 g/m. Mchugh (1983) used a Plexiglas cylinder sample on Φ 300×300 mm, the PETN charges had diameters of 3.2 mm (4 g/m). Banadaki and Mohanty (2012) experimented with cubic samples (150×150×150 mm), and the diameters of PETN cylindrical charges were 1.1~2.23 mm (1.2~5.3 g/m). Rathore and Bhandari (2007) tested blasts in limestone blocks (550×300×250 mm) at the laboratory scale by using the detonating cord with 8.5 g/m.

Based on the above research results, the specimen consists of two parts (A and B), each part is 200 mm in diameter and 50 mm long. The strain sensors were pasted on one face of A and another face was used for HS test,

and B was used to remove reflected waves in the strain sensor surface (Figure 6). Five strain gages were pasted with a spacing of 12 mm, and the nearest gage was located on 28 mm. The center borehole was drilled on 10 mm in diameter. The distance between the DIC surface and the hole bottom was 10 mm. The PETN Charge and detonation cord were used for one-time loading and cyclic loading in experiment, as shown in Table 1. The copper tube with 1.5 mm thick was tightly installed in the borehole to prevent explosion gas penetrating into fissure.

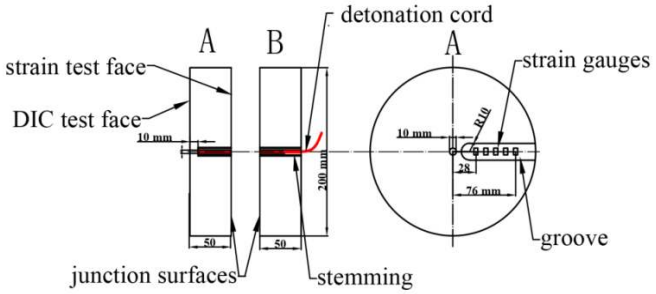

Figure 6: Schematic diagram of sample.

Table 1: Parameters of two detonations.

Detonation	Diameter (mm)	Density (g/cm^3)	Linear density (g/m)	VOD (m/s)
PETN Charge	2.80	1.0	6.15	6500
PETN Cord	1.98	1.3	4.00	6850

In this study, six groups of specimens were performed in the Laboratory of Explosion at the Beijing Institute of Technology. Tests 1~3 were conducted to study the failure process under blast loading with different confining pressures (0 MPa, 5 MPa and 10 MPa). Tests 4~6 were to investigate the effects of cycle-index on damage accumulative evolution under cyclic blast loadings. The electric discharge method was used to inspire the synchronization trigger system. The specimens in tests 4~6 were failure completely after 3, 4, 5 loadings, respectively, as shown in Table 2.

Table 2: Parameters of six tests.

Test	Radius (mm)	Length (mm)	Diameter of borehole (mm)	Length of hole (mm)	Confining pressure (MPa)	Detonation Cord	Loading times
1	100.25	50.55	10.10	41.15	0	PETN Charge	1
2	99.60	49.35	10.20	40.95	5	PETN Charge	1
3	101.00	49.30	10.35	42.00	10	PETN Charge	1
4	99.85	49.75	10.00	40.15	0	Detonation cord	3
5	99.90	49.55	10.00	40.90	5	Detonation cord	4
6	101.05	49.90	10.15	41.00	10	Detonation cord	5

The strain gauges require a DC power supply and a Wheatstone bridge for signal amplification. The strains were calculated by the voltage signal. The deformation signals were recorded by LTT24-Messsystem on 4 MS/s. The high-speed stereo-vision system consisting of a Fastcam SA5 high-speed camera, VIC-2D software ver.7, lenses and optical lenses with different focal lengths were used in experiment. The array size was 384×344, and 2,000-W halogen lamps were used to provide sufficient light intensity for improving the sharpness of the photos. The speed of the high-speed camera was 50,000 frames/s, the interval time between two photographs was 20 μs. The HS test surface and parameters about camera was given in Figure 7. In order to describe the key points and specimen in different perspectives, the photographs in experiment were given in Figure 8.



Figure 7: Parameters of high-speed camera.

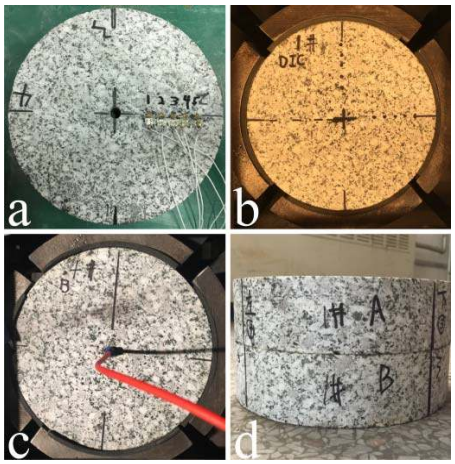

Figure 8: Photographs of specimen. (a) Strain test surface, (b) HS test surface, (c) Detonation cord, (d) Two parts.

3. RESULTS AND DISCUSSION

3.1 Dynamic response under one-time loading

Three stages were clearly found in strain-time curve after detonation (Figure 9). The first high frequency oscillation represented the strain signal was influenced by the ionization interference during detonating, and it last 70 μs. The second part was the dynamic deformation of rock under stress wave by blasting, and it last 30 μs. The propagation velocity of stress wave is 3738 m/s in rock sample, the test points at different position almost rose up at 150 μs. When incident stress wave spread to the free boundary of sample, the reflected waves was produced and the strain rose again under the secondary loading. The explosion gases loading was ignored because the copper tube can prevent gas flowing into fissures.

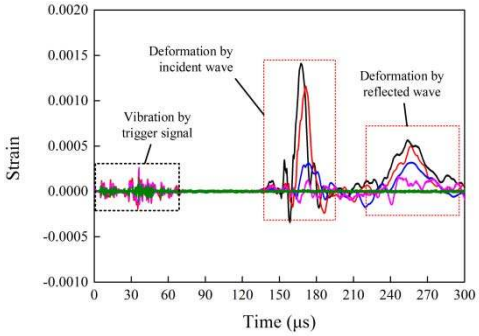

Figure 9: Three stages in strain-time curve after blasting.

The yield strength of rock under blasting is higher than it in SHPB experiment (the rock material become stronger with strain rates increase). The material around borehole is crushed by extremely high pressure (with higher strain), and the damage zone away from borehole is produced by tensile failure (with lower strain). The tensile strength from SHPB results are used as the failure criteria when analyze the failure process by hoop tensile in the explosion experiment. The average strain (0.002) on the descending part of tensile stress-strain curve is selected as the fracture strain, and the peak strain (0.0005) on linear part is used as the ultimate elastic strain.

Figure 10 shows the hoop strain-time in test 2. The strain on SD 1 rose up to 0.0046 at 190 μs, it exceeded the tensile failure strain and micro fissures were produced near borehole. Then the deformation sharply decreased as stress wave propagated, the strain peaks of SD 4~5 were less than 0.002, and more dates were collected in Table 3.

The attenuation of tensile strain is plotted in Figure 10 under different confining pressures. When the confining pressure was 0 MPa, the strain on 30 mm exceeded 0.007, the damage and fissures were formed by shear and tensile failure. With confining pressure increased to 5 MPa, the strain reduced 0.0046, the plastic deformation in the damage zone was weakened gradually. The strain was linear attenuated with distance increased. When the confining pressure was 10 MPa, the elastic deformation played a dominating role during blasting, and the confining pressure reduced the tensile failure by shock wave.

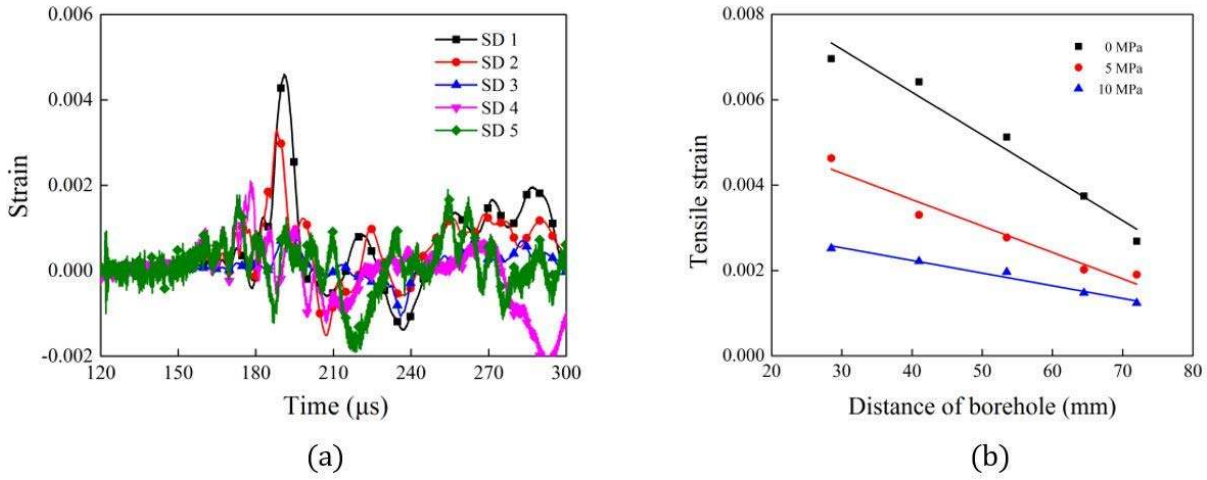

Figure 10: (a) Strain-time curve under 5 MPa confining pressure; (b) Attenuation of tensile strain.

Table 3: Peak strain under different confining pressures.

Test	SD1	SD2	SD3	SD4	SD5
1	0.0070	0.0064	0.0051	0.0037	0.0027
2	0.0046	0.0033	0.0027	0.0021	0.0019
3	0.0025	0.0022	0.0020	0.0015	0.0012

Using the strain gages with a higher sampling rate can capture the deformation of rock by stress wave, and HS technique is more easily to observe crack growth due to the crack propagation speed is less than stress wave. Figure 11 clearly displays the evolution of strain field on the HS test surface under different confining pressures, and the interval between adjacent photos is 20 μs. The time shown in the top right corner is started at the deformation of specimen. Initial stress wave from borehole propagated along the radial direction at 0~40 μs. The pressure of stress wave gradually was decreased in propagation. When the initial stress wave arrived boundary at 40 μs, the reflected stress wave were produced and strain concentration appeared on the upper edge. The strain concentration band extended to the boundary at 160 μs.

Under the condition of no confining pressure, the strain concentration zone was about five times borehole's diameter at 100 μs. The average strain in damage area was 0.01 and exceeded the material failure strength. The small cracks were appeared in central zone inevitably. Two radial cracks grow from the central damage zone and developed along radial direction, one run through sample and another stopped on 20 mm. The reflected tensile wave from boundary drove the radial crack growing. When the confining pressure increased to 5 MPa, the broken zone radius reduced obviously. Four strain concentration bands were formed at 100 μs, and none extended to the border finally because the confining pressure reduced the hoop tensile fracture. When the confining pressure rose to 10 MPa, the radius of broken zone further reduced and radial cracks were not formed. The expansion gases

together with detonation products overflowed from the bottom at 100 μs, more explosive energy escaped from the central zone. The tensile failure by shock wave was gradually decreased as confining pressure increased.

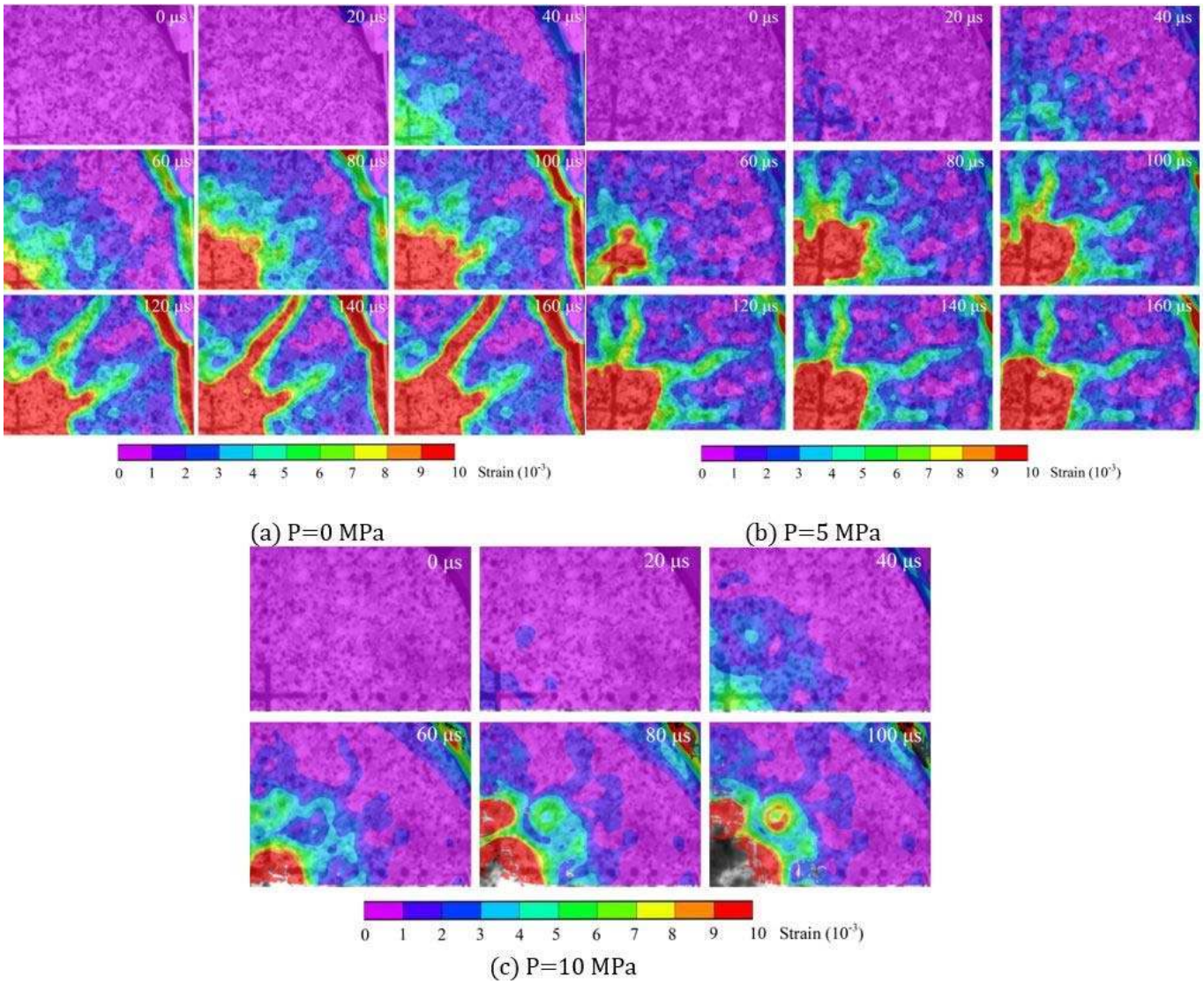

Figure 11: Crack propagating process under different confining pressures.

Figure 12 and Figure 13 list the distribution of damage on two surfaces of A part under three confining pressures in experimental results. The shape feature of cracks on the free surface is the same as the DIC analysis results. Three visible radial cracks are produced and the biggest one is 1.5 mm in width (located on the left side in Figure 12a). As shown in Figure 12b, only one macroscopic crack appears in the lower right area under 5 MPa pressure. When the confining pressure increases to 10 MPa, no obvious cracks were found (Figure 12c). Note that the width of crack is increased with crack growing. In the strain gauge test surface, the radius of broken zone is 40 mm, 32 mm, 15 mm corresponding to 0 MPa, 5 MPa and 10 MPa confining pressure, respectively (Figure 13). The circumference compressive pre-stress from confining pressure would prevent the radial crack propagating and reduced the broken area.



Figure 12: Crack distribution on free surface under 0 MPa, 5 MPa, 10 MPa.

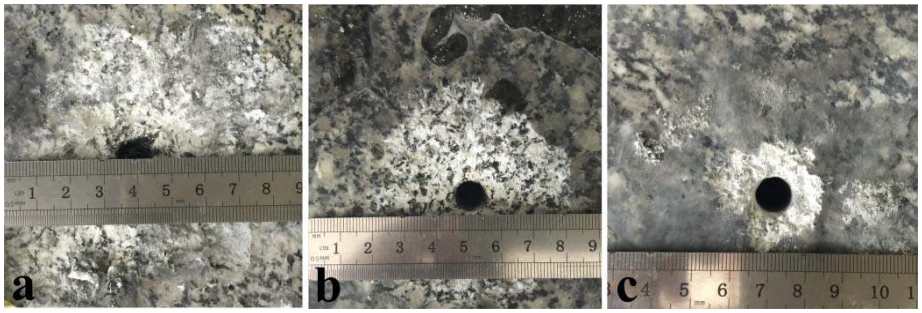

Figure 13: Broken zone on strain gauge surface under 0 MPa, 5 MPa, 10 MPa.

A micro crack in the damage zone is observed by SEM with different magnifications, as shown in Figure 14. A horizontal crack develops along the meander line and stop on the boundaries of mineral particles. In the vicinity of the crack surfaces, the fragmented rocks are generated and the intergranular cracking occurred under the dynamic loading.

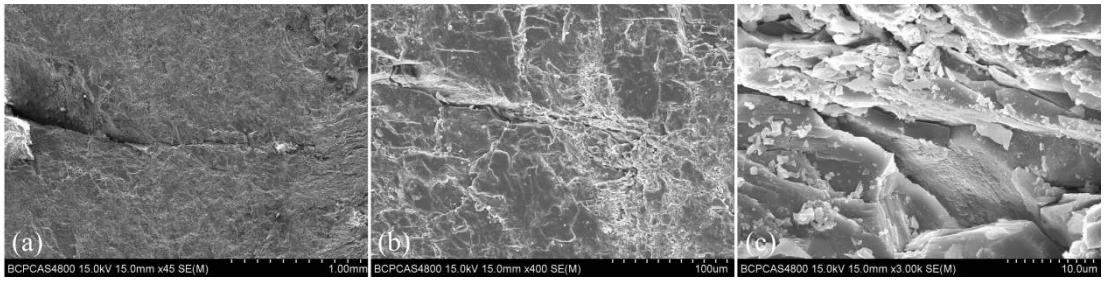

Figure 14: SEM micrographs of fracture surfaces. (a) SEM on 1 mm. (b) SEM on 100 μm. (c) SEM on 10 μm.

3.2 Dynamic response under cyclic loadings

The rock specimens were failed completely after 3, 4, 5 loadings in text 4~6, respectively. The strain-time in test 5 after four blasting was plotted (Figure 15). After the first loading, the strain peak of SD 1and SD 2 arrived 0.001 and less than the failure tensile strain. Strain decreased with stress wave propagated, and the elastic deformation played a dominant role under first loading. The strain curve by second loading was similar with the first results, the strain on SD 1 and SD 2 exceeded 0.001. The deformation increased by reflected wave at 240~270 μs. When the specimen subjected third loading, strain on SD 1 rose up to 0.0015 and exceed tensile strength. The irreversible damage was produced by plastic deformation, and the micro fractures appeared around the borehole. Meanwhile strain of SD 3 increased to 0.0004, and damage accumulation was improved after cyclic loadings. After the last loading, rock samples was broken and the strain on SD 2 was infinite due to strain exceeded the range of measurement for gauges. The strain peaks of other points were more than 0.001 and did not fall back to zero at last. The existing flaws or radial cracks would further develop, and run through specimen after the last loading.

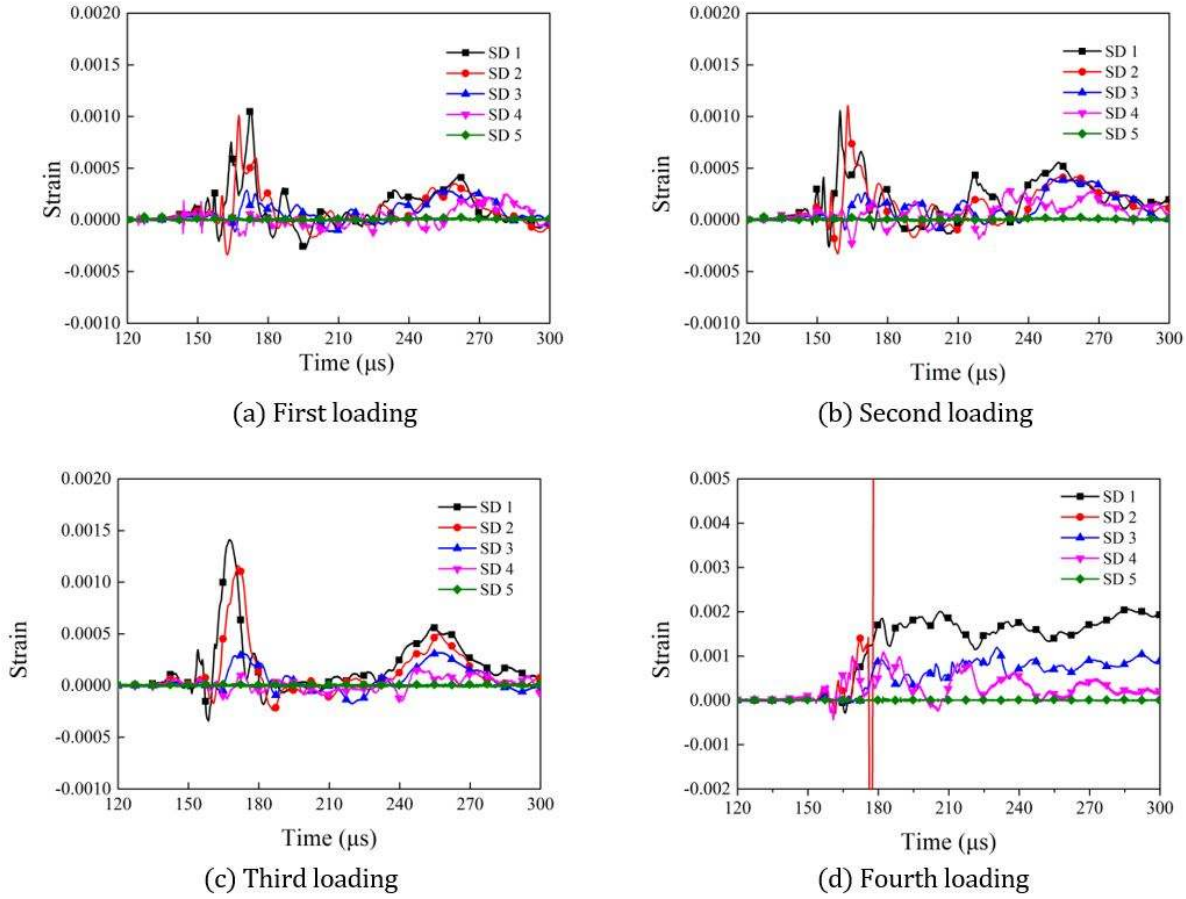

Figure 15: Strain-time curve of target points with 5 MPa pressure under cyclic loadings.

Table 4 lists the strain peaks during 150 μs~300 μs in test 4~6, and specimens are failure after 3, 4, 5 loadings, respectively. "--" represents the strain data is not recorded.

Table 4: Strain peak in test 4~6 under cyclic loadings.

Test	4			5				6				
Cyclic loadings	L 1	L 2	L 3	L 1	L 2	L 3	L 4	L 1	L 2	L 3	L 4	L 5
SD 1	0.0017	0.0026	0.0057	0.0010	0.0011	0.0014	0.0021	0.0009	0.0012	0.0015	0.00291	0.0142
SD 2	0.0015	0.0019	0.0041	0.0011	0.0010	0.0012	0.0085	0.0009	0.0010	0.0011	0.0016	0.0064
SD 3	0.0006	0.0013	0.0032	0.0003	0.0002	0.0004	0.0012	0.0001	0.0002	0.0003	0.0009	0.0060
SD 4	0.0011	0.0015	0.0030	0.0001	0.0003	0.0002	0.0011	0.0001	0.0001	0.0002	0.0020	0.0056
SD 5	0.0023	0.003	0.0050	--	--	--	--	0.0008	0.0022	0.0041	0.0078	--

Figure 16 presents the deformation accumulation under cyclic loadings. The strain peak rose with loading times, and the deformation was largest without boundary constraint. As shown in Figure 16a, the deformation on SD 5 was bigger than other points. This phenomenon was ascribed to the tensile fracture by reflected wave. After the third loading, the neatest point SD 1 rose up to 0.006 and the irreversible failures have been produced.

When confining pressure was 5 MPa, the average strain was smaller than the results in unrestrained conditions. The circumference pre-stress field was produced by initial confining pressure, and it reduced the tensile failure by blast loading (Figure 16b). The stain peaks on SD 1 and SD 2 were much bigger than SD 3 and SD 4, the plastic deformation caused the crushing zone close to bore hole. As the confining pressure rose up to 10 MPa, specimen was fractured after five loadings (Figure 16c). Elastic deformation was produced under the former loadings, and then strain increased rapidly under the last loading and the brittle fracture caused the failure of rock.

Because the reflected wave had little effect on deformation in the middle zone, the SD 3 was selected to explored damage accumulation process. As shown in Figure 16d, when the confining pressure increased from 0 MPa to 5 MPa, the tensile failure from the shock wave reduced. This tendency is not significantly as confining pressure rose up to 10 MPa. Elastic distortion and accumulated damage were not obviously under earlier cyclic loadings, and then became seriously after plastic deformation appeared.

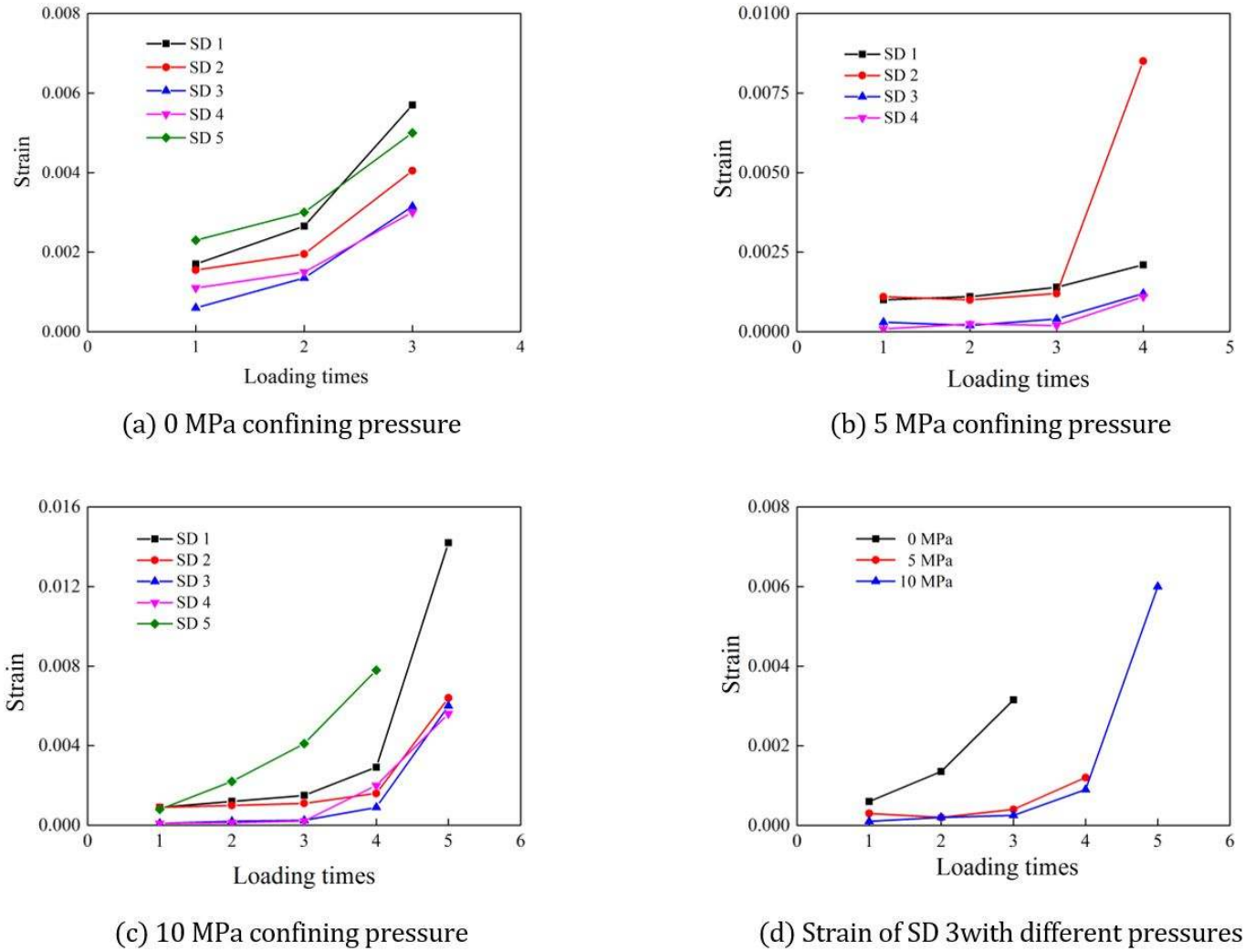

Figure 16: Strain field under cyclic loadings.

Rathore and Bhandari (2007) established the elastic damage coupled with crack propagations in strain space based on continuum media theory, the damage of rock is calculated by plastic strain. At first loading, the rock material is mainly controlled by elastic deformation and no damage appeared. When the strain peak exceeds the elastic limit strength of rock, the accumulation of plastic strain increases and the permanent deformations are generated. At last, the plastic strain reach the fracture strain (ε_f) and the material is damaged completely. When the plastic deformation happened in the material, the damage can be calculated as:

$$\begin{cases} D = 0 & (\varepsilon_p < \varepsilon_e) \\ D = \dfrac{\varepsilon_p}{\varepsilon_f} & (\varepsilon_p > \varepsilon_e) \\ D = 1 & (\varepsilon_p > \varepsilon_f) \end{cases} \qquad (1)$$

Where D represents damage, ε_p is the strain peak, ε_e is the ultimate elastic strain, ε_f is fracture strain. According to the SHPB experimental results, $\varepsilon_e = 0.0005,\ \ \varepsilon_f = 0.002.$

The process of damage accumulation under cyclic blasting in test 5 is listed in Figure 17. Under the first loading, the damage near the borehole was more than 0.4 and micro fractures were produced by plastic deformation. As loading times increased, the accumulation of damage was observably within 40 mm from explosive source, and the further zone (beyond 50 mm) was mainly controlled by elastic deformation. After the forth loading, the damage value on 42 mm increased from 0.6 to 1.0 and rock material was complete failure. The results illustrated that the damage accumulation nonlinearly increased under cyclic loadings.

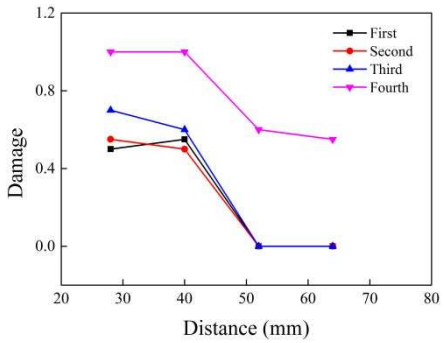

Figure 17: Damage accumulation under cyclic loadings in test 5.

Figure 18 displays the evolution of the Mises strain field in test 4. After the first loading, the maximum strain was 0.002 at 160 μs in the central zone with 10 mm in radius. The deformation along boundary became seriously when the initial shock wave arrived the free boundary. The average strain of central region was lower than 0.0006, and the elastic deformation played a dominant role during first loading. After the second loading, the strain around the borehole reached 0.005, and the radius of damage zone increased to 25 mm. A few strain bands were generated and the plastic deformation drove macro cracks growing. The fracturing process was clearly shown in Figure 18 after the last loading, the strain peak exceeded the elastic limit of rock material. The crushing grains together with detonation products escaped from the bottom of borehole at 120 μs, many radial cracks developed and the existing cracks would extended further under reflected extension waves.

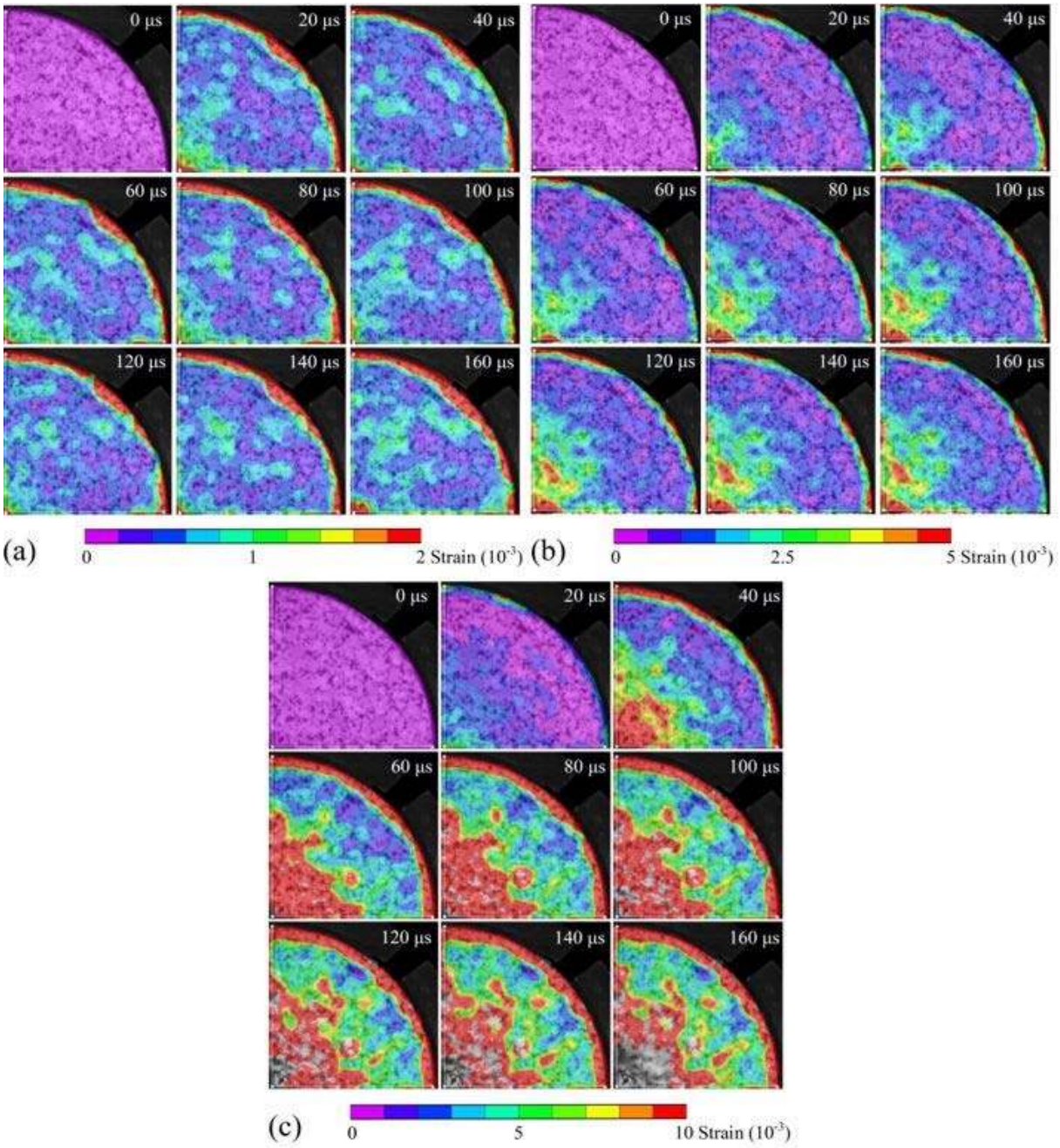

Figure 18: Crack propagating process of rock in test 4. (a) First loading, (b) Second loading, (c) Third loading.

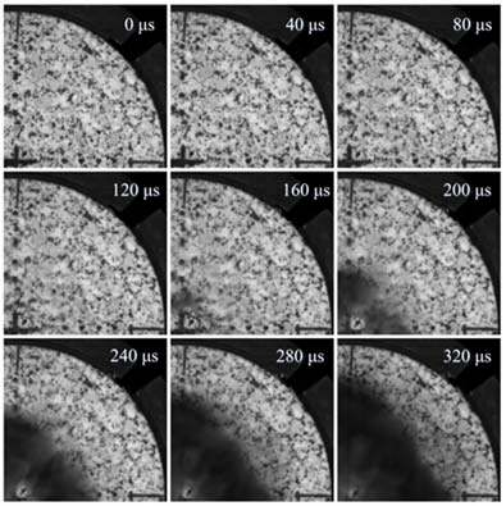

Figure 19: Specimen failure process in Test 4.

Figure 19 clearly exhibits the failure process in test 4 under the third blast loading. The deformation were produced by stress waves before 160 μs, then the-explosion gases with high pressure and temperature flowed out from central borehole during 160 μs~320 μs. The deformation cannot be analyzed in the later stage due to the explosive gases reduced the sharpness of the photos.

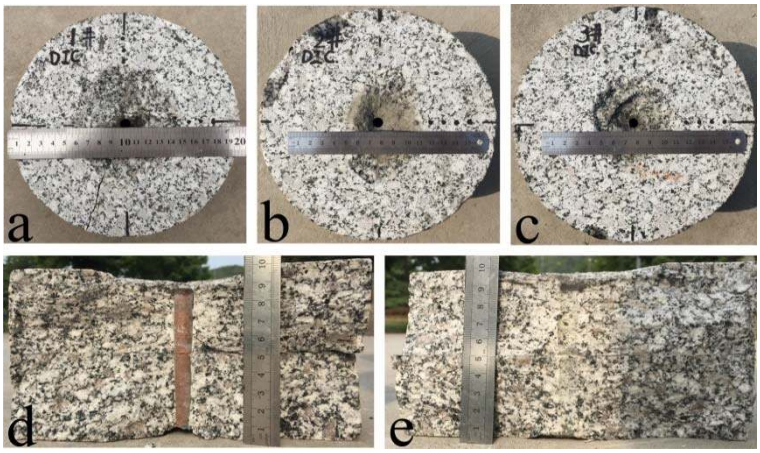

Figure 20: Crack distribution. (a) Test 4; (b) Test 5; (c) Test 6; (d) (e) Damage pattern of test 5 on longitudinal profile.

Figure 20 shows the fractures and damage pattern in three tests by experimental photographs. The diameter of central damage area was 100 mm in test 4, the collapses phenomenon caused by the reflected tension wave was seriously. Two visible radial cracks appeared in vertical direction and ran thought specimen, the width of bigger one was 2 mm (Figure 20a). As shown in Figure 20b, the central damage area decreased to 40 mm in diameter because the initial confining pressure (5 MPa) reduced the circumference tensile failure. Only one fissure can be observed in the top right corner. When confining pressure rose up to 10 MPa, the central damage zone was not extended, one indistinct radial crack located on the top left corner (Figure 20c). As shown in Figure 20d and Figure 20e, the copper tube was not destructed after four blast loadings and the wall of borehole was smooth. The results indicated the explosion gas products did not flow into the junction surface, and the strain signals from strain gages were mainly caused by stress wave. Notably, the spallation was observably on the top and bottom surfaces, and the phenomenon was caused by the combined action of the initial wave and reflected tension wave.

4 CONCLUSIONS

Laboratory study was performed to investigate the deformation characteristic of rock subjected to active confining pressure and cyclic blasting. Based on the advantage of natural granite textures, HS and strain

measurement techniques were used to observe the crack propagation and test the dynamic deformation under different confining pressures, respectively.

Under the one-time loading from PETN cylindrical charge with a small diameter, cracks around borehole were generated by shear and tensile failure under the extreme pressure. The radial cracks were primarily produced by circumferential tensile stress from shock wave. Circumference compressive stress was produced by confining pressure, and it reduced the tensile failure by explosive loading. The number and size of radial cracks reduced significantly with confining pressure increase from 0 MPa to 10 MPa. With the distance increase, the strength of explosion shock wave reduced and confining pressure prevented cracks from growing.

When rock subjected to cyclic loadings from PETN Cord, the specimen was controlled by elastic deformation and no damage appeared after the first loading. Then the accumulation of plastic strain increased when strain exceeded the elastic limit strength of rock. Damage slowly increased with cycle-index increased, the damage increased sharply and specimen failure completely after the last loading. The damage accumulation was nonlinear increased as loading times increased, and the existing flaws or radial cracks further extend under cyclic loading and ran through specimen finally.

Notice that the micro cracks developed along the meander line and intergranular cracking occurred under the dynamic loading, the microstructures were observed in the SEM results.

References

Bagde, M. N., & Petroš, V. (2005). Fatigue properties of intact sandstone samples subjected to dynamic uniaxial cyclical loading. *International Journal of Rock Mechanics & Mining Sciences*, *42*(2), 237-250.

Banadaki, M. M. D., & Mohanty, B. (2012). Numerical simulation of stress wave induced fractures in rock. *International Journal of Impact Engineering*, *40*(2), 16-25.

Brown, E. T., & Hoek, E. (1978). Trends in relationships between measured in-situ stresses and depth. *International Journal of Rock Mechanics & Mining Sciences & Geomechanics Abstracts*, *15*(4), 211-215.

Cho, S. H., & Kaneko, K. (2004). Influence of the applied pressure waveform on the dynamic fracture processes in rock. *International Journal of Rock Mechanics & Mining Sciences*, *41*(5), 771-784.

Eason, G. (1963). Propagation of waves from spherical and cylindrical cavities. *Zeitschrift Für Angewandte Mathematik Und Physik Zamp*, *14*(1), 12-23.

Ge, X., Yu, J., Lu, Y., & Ren, J. (2003). TESTING STUDY ON FATIGUE DEFORMATION LAW OF ROCK UNDER CYCLIC LOADING. *Chinese Journal of Rock Mechanics & Engineering*, *22*(10), 1581-1585.

Guo, Y. T., Zhao, K. L., Sun, G. H., Yang, C. H., Hong-Ling, M. A., & Zhang, G. M. (2011). Experimental study of fatigue deformation and damage characteristics of salt rock under cyclic loading. *Rock & Soil Mechanics*, *32*(5), 1353-1359.

Jin, J. F., Xi-Bing, L. I., Yin, Z. Q., & Kun, D. U. (2012). Effects of axial pressure and number of cyclic impacts on dynamic mechanical characteristics of sandstone. *Journal of China Coal Society*, *37*(6), 923-930.

Li, H., Xiang, X., Li, J., Jian, Z., Bo, L., & Liu, Y. (2011). Rock damage control in bedrock blasting excavation for a nuclear power plant. *International Journal of Rock Mechanics & Mining Sciences*, *48*(2), 210-218.

Lin, D. N., Chen, S. R., & Liu, Y. P. (2005). Experimental Study on Confining Pressure Effect of Rock Damage Under Cyclical Impact Loading. *Mining & Metallurgical Engineering*, *25*(4), 12-15.

Liu, E. L., He, S., Xue, X., & Xu, J. (2011). Dynamic Properties of Intact Rock Samples Subjected to Cyclic Loading under Confining Pressure Conditions. *Rock Mechanics & Rock Engineering*, *44*(5), 629-634.

Liu, J., Xie, H., Xu, J., & Yang, C. (2008). Experimental study on damping characteristics of rock under cyclic loading. *Chinese Journal of Rock Mechanics & Engineering*, *27*(4), 712-717.

Ma, L. J., Liu, X. Y., Wang, M. Y., Xu, H. F., Hua, R. P., Fan, P. X., . . . Yi, Q. K. (2013). Experimental investigation of the mechanical properties of rock salt under triaxial cyclic loading. *International Journal of Rock Mechanics & Mining Sciences*, *62*(9), 34-41.

Mchugh, S. (1983). Crack extension caused by internal gas pressure compared with extension caused by tensile stress. *International Journal of Fracture*, *21*(3), 163-176.

Onederra, I. A., Furtney, J. K., Sellers, E., & Iverson, S. (2013). Modelling blast induced damage from a fully coupled explosivecharge. *Int J Rock Mech Min Sci*, *58*(58), 73-84.

Ramulu, M., Chakraborty, A. K., & Sitharam, T. G. (2009). Damage assessment of basaltic rock mass due to repeated blasting in a railway tunnelling project – A case study. *Tunnelling & Underground Space Technology*, *24*(2), 208-221.

Rathore, S. S., & Bhandari, S. (2007). Controlled Fracture Growth by Blasting While Protecting Damages to Remaining Rock. *Rock Mechanics & Rock Engineering*, *40*(3), 317-326.

Simha, K. R. Y., Fourney, W. L., & Dick, R. D. (1984). Studies On Explosively Driven Cracks Under Confining In-Situ Stresses.

Wang, P., Xu, J., Liu, S., & Wang, H. (2016). Dynamic mechanical properties and deterioration of red-sandstone subjected to repeated thermal shocks. *Engineering Geology*, *212*, 44-52.

Zhang, Q. B., & Zhao, J. (2014). A Review of Dynamic Experimental Techniques and Mechanical Behaviour of Rock Materials. *Rock Mechanics & Rock Engineering*, *47*(4), 1411-1478.

Zhou, W. (1998). Elasto brittle damage model for rockmass based on field tests in Laxiwa arch dam site. *Chinese Jounal of Geotechnical Engineering*.

Latin American Journal of Solids and Structures
www.lajss.org

Erratum

In the article **Laboratory study of dynamic mechanical characteristic of granite subjected to confining pressure and cyclic blast loading**, doi number: https://doi.org/10.1590/1679-78254424, published in journal Latin American Journal of Solids and Structures, 15(5):e44, page 1:

Where it reads:

Chenglong He[a]

Jun Yang[a]*

[a] State Key Laboratory of Explosion Science and Technology, Beijing Institute of Technology, Beijing, China. E-mail: hechenglong@bit.edu.cn, yangj@bit.edu.cn

* Corresponding Author

It should read:

Chenglong He[a]*

Jun Yang[b]

[a] College of Mechatronics Engineering, North University of China, Taiyuan 030051, China. E-mail: hechenglong@bit.edu.cn

[b] State Key Laboratory of Explosion Science and Technology, Beijing Institute of Technology, Beijing, China. E-mail: yangj@bit.edu.cn

* Corresponding Author

(cc) BY